Physics in Medicine & Biology

PAPER • OPEN ACCESS

Supine MRI for regional breast radiotherapy: imaging axillary lymph nodes before and after sentinel-node biopsy

To cite this article: Tristan C F van Heijst *et al* 2017 *Phys. Med. Biol.* **62** 6746

OPEN ACCESS
IOP Publishing | Institute of Physics and Engineering in Medicine Physics in Medicine & Biology
Phys. Med. Biol. **62** (2017) 6746–6761 https://doi.org/10.1088/1361-6560/aa759f

Supine MRI for regional breast radiotherapy: imaging axillary lymph nodes before and after sentinel-node biopsy

Tristan C F van Heijst[1,7], Debora Eschbach-Zandbergen[1,8], Nienke Hoekstra[2,8], Bram van Asselen[1], Jan J W Lagendijk[1], Helena M Verkooijen[3], Ruud M Pijnappel[4], Stephanie N de Waard[4], Arjen J Witkamp[5], Thijs van Dalen[6], H J G Desirée van den Bongard[1] and Marielle E P Philippens[1]

[1] Department of Radiotherapy, University Medical Centre Utrecht, Utrecht, Netherlands
[2] Department of Radiation Oncology, Erasmus Medical Centre, Rotterdam, Netherlands
[3] Department of Epidemiology, University Medical Centre Utrecht, Utrecht, Netherlands
[4] Department of Radiology, University Medical Centre Utrecht, Utrecht, Netherlands
[5] Department of Surgery, University Medical Centre Utrecht, Utrecht, Netherlands
[6] Department of Surgery, Diakonessenhuis Hospital, Utrecht, Netherlands

E-mail: t.c.f.vanheijst@umcutrecht.nl

Received 29 December 2016, revised 11 May 2017
Accepted for publication 30 May 2017
Published 1 August 2017

Abstract

Regional radiotherapy (RT) is increasingly used in breast cancer treatment. Conventionally, computed tomography (CT) is performed for RT planning. Lymph node (LN) target levels are delineated according to anatomical boundaries. Magnetic resonance imaging (MRI) could enable individual LN delineation. The purpose was to evaluate the applicability of MRI for LN detection in supine treatment position, before and after sentinel-node biopsy (SNB). Twenty-three female breast cancer patients (cTis-3N0M0) underwent 1.5 T MRI, before and after SNB, in addition to CT. Endurance for MRI was monitored. Axillary levels were delineated. LNs were identified and delineated

[7] Department of Radiotherapy, University Medical Centre Utrecht, HP: Q00.118, Heidelberglaan 100, 3584CX Utrecht, Netherlands.
[8] These two authors contributed equally to this work.

on MRI from before and after SNB, and on CT, and compared by Wilcoxon signed-rank tests. LN locations and LN-based volumes were related to axillary delineations and associated volumes. Although postoperative effects were visible, LN numbers on postoperative MRI (median 26 LNs) were highly reproducible compared to preoperative MRI when adding excised sentinel nodes, and higher than on CT (median 11, $p < 0.001$). LN-based volumes were considerably smaller than respective axillary levels. Supine MRI of LNs is feasible and reproducible before and after SNB. This may lead to more accurate RT target definition compared to CT, with potentially lower toxicity. With the MRI techniques described here, initiation of novel MRI-guided RT strategies aiming at individual LNs could be possible.

Keywords: MRI, breast cancer, lymph nodes, radiotherapy, MRI guidance, sentinel-node biopsy

(Some figures may appear in colour only in the online journal)

1. Introduction

In recent years, regional treatment for breast cancer patients with tumour-positive sentinel nodes (SNs) has changed. Regional radiotherapy (RT), performed after breast-conserving surgery (BCS) or mastectomy, is increasingly used as an alternative to axillary lymph node (LN) dissection (Giuliano *et al* 2010, Galimberti *et al* 2013, Donker *et al* 2014). In conventional regional breast RT, target volumes are contoured on computed tomography (CT) scans, according to contouring guidelines, including those recently published by the European Society for Radiotherapy and Oncology (ESTRO) (Offersen *et al* 2015). These guidelines focus on the delineation of axillary levels based on vessels and muscles, since LN visibility on CT is limited. Furthermore, the location of regional LNs varies greatly between patients (Dijkema *et al* 2004). Magnetic resonance imaging (MRI) can image individual axillary LNs better (Lernevall 2000, Harnan *et al* 2011, Rahbar *et al* 2012, Ahmed *et al* 2014, Li *et al* 2014, Menezes *et al* 2014, Kuijs *et al* 2015) in direct relation to surrounding anatomical structures, e.g. the brachial plexus, heart, and chest wall. Anatomical information on exact LN locations obtained from dedicated MRI techniques may lead to adapted regional breast RT target volumes, such that more healthy tissue can be spared. This could result in decreased RT-related toxicity, consisting of arm morbidity, e.g. pain, edema, and shoulder stiffness. To our knowledge, this has not been investigated previously.

Conventional diagnostic breast MRI is not optimized for RT planning, and is acquired in prone position. We have previously developed dedicated MRI, in healthy volunteers, to image axillary LNs for RT planning in supine treatment position (van Heijst *et al* 2016). Both anatomy and posture endurance in patients undergoing MRI are likely to differ from that of healthy volunteers (Luscieti *et al* 1980, Hadamitzky *et al* 2010). The next step is, therefore, to validate MRI for regional RT in breast cancer patients who are scanned in a treatment position.

In standard elective RT, entire axillary LN levels are irradiated. Using MRI, LNs could potentially be delineated and targeted individually. This makes the reproducibility of detecting LNs of the utmost importance. Furthermore, LN identification on MRI may be affected by axillary surgery. This is usually limited to sentinel-node biopsy (SNB), which is performed for staging purposes, in combination with breast surgery. The surgical excision of one or more SNs in SNB leads to anatomical alterations, potentially also due to inflammation and seroma

formation (Srivastava *et al* 2012). Moreover, patient posture endurance for undergoing MRI may be affected by surgery.

The purpose of this work is to test the reproducibility of LN detection using MRI, and posture endurance, in breast cancer patients who undergo SNB, pre- and postoperatively, in supine treatment position. Furthermore, anatomical locations and volumes of all LNs, including SNs excised during SNB, are related to the standard delineation of axillary levels. LN detection rates of MRI are compared to standard postoperative CT.

2. Materials and methods

2.1. Patients

The Internal Review Board of University Medical Center (UMC) Utrecht approved the study, which is registered under Netherlands trial number NL50046.041.14. Written informed consent was obtained from 23 female patients (table 1), who were diagnosed with either ductal carcinoma *in situ* (DCIS), or early-stage breast cancer without pathologically involved LNs or distant metastasis (cTis-T3N0M0). They were scheduled for SNB, performed during BCS or mastectomy, at UMC Utrecht or at Diakonessenhuis Hospital, in Utrecht, The Netherlands. No surgery or RT had been performed previously in the ipsilateral axilla. One patient underwent mastectomy, while 22 participants underwent BCS, 21 of whom received subsequent standard RT treatment at UMC Utrecht.

2.2. MRI set-up

Scanning was performed on a 1.5 T wide-bore MRI scanner (Philips Ingenia, The Netherlands) at the RT Department of UMC Utrecht, from February 2015 until February 2016. Participants were scanned in supine RT position (van Heijst *et al* 2016), i.e. with arms in abduction, supported by a wedge-board (Thorawedge, CIVCO Medical Solutions, The Netherlands). An anterior receive coil was connected and placed on an adjustable polymethyl-metacrylate support, such that the outer anatomy was not deformed. A posterior receive coil was located in the scanner table.

2.3. MRI and CT scanning

Participants underwent two MRI scan sessions. The first was performed a median 7 d (range: 1–23 d) before surgery, whereas the second took place a median 20 d (range: 8–45 d) after surgery. Five MRI scans were acquired on both occasions, which were optimized previously in healthy volunteers (van Heijst *et al* 2016). Relevant imaging parameters are listed in table 2. No contrast agent was administered.

The first method was a T1-weighted (T1w) spoiled gradient echo (SPGR) technique, acquired transversally. The in-plane field of view (FOV) encompassed the outer body contour, ranging in the cranial-caudal direction from the mandible to the caudal border of the breast. Here, multi-point Dixon (mDixon) water-fat separation was applied, where two echoes are used to separate signal from fat and water (Eggers *et al* 2011). The other four MRI scans were acquired in the coronal plane, with FOVs covering the axillary areas. One MRI technique was a T1w SPGR sequence using mDixon, with a smaller FOV than the first T1w SPGR, but higher in resolution. Furthermore, two-dimensional (2D) and 3D T2w fast spin echo techniques were both applied. The final scan was a diffusion-weighted MRI (DWI), in which restriction of water mobility is reflected by hyper-intense signal.

Table 1. Patient characteristics for the 23 participants included in our study.

Variable		$n = 23$
Age (years)	Range	40–80
	Median	58
BMI (kg m^{-2})	Range	18.3–34.5
	Median	24.0
Affected breast	Left	11 (48%)
	Right	12 (52%)
Tumour stage		
Clinical	cTis	3 (13%)
	cT1	18 (78%)
	cT2	2 (9%)
Pathological	pTis	3 (13%)
	pT1	17 (74%)
	pT2	3 (13%)
Nodal stage		
Clinical	N0	23 (100%)
Pathological	N0(sn)	21 (91%)
	N1(sn)	2 (9%)

Note: BMI = body mass index; sn = sentinel node.

Twenty-one patients underwent postoperative CT imaging for standard RT planning in supine RT position, on a support (CIVCO, The Netherlands). This was usually performed on the same day as postoperative MRI. Acquisition duration was 20 s, slice thickness 3 mm, and minimal in-plane resolution was $1 \times 1\,\text{mm}^2$ (Brilliance, Philips). The FOV of the RT-planning CT included the breast and axillary regions.

2.4. Posture endurance for MRI

Acquisition time of MRI was limited to 20 min per session. With the additional time needed for positioning and scanner preparation, the supine RT position had to be maintained for up to 30 min in each session. Since this is potentially difficult to endure, we monitored whether the patient was able to finish the procedure. If applicable, the reason for the insufficient posture endurance was recorded, as was the need for any adjustments in positioning.

2.5. Contouring of axillary levels on MRI

The first T1w scan, with the largest FOV, was considered as the reference scan, to which other scans of the same MRI session were co-registered. This was performed by a rigid registration, based on anatomical reference structures (e.g. large blood vessels or muscles) which were not close to the SNB location. Since automatic cross-contrast registration algorithms are complex and prone to error, this was performed manually. For MRI methods using mDixon, water-only (Dixon-water) and fat-only (Dixon-fat) images were both examined. A breast radiation oncologist contoured standard regional target volumes on preoperative scans (figure 1), according to ESTRO delineation guidelines (Offersen *et al* 2015). These were developed for CT, but are

Table 2. Imaging parameters of the MRI sequences used for LN imaging in this study. The 3D scans were reconstructed using overcontiguous slices.

Sequences imaging parameters	T1-TFE (reference)	T2-TSE	T2-VISTA	DWI	T1-FFE
Type of sequence	TFE	TSE	TSE	EPI	FFE
Weighting	T1	T2	T2	Diffusion	T1
Fat suppression/ separation	mDixon	mDixon	SPAIR	STIR	mDixon
Dimensionality	3D	2D	3D	2D	3D
Acquisition plane	Transverse	Coronal	Coronal	Coronal	Coronal
Acquired resolution	$1.50 \times 1.50 \times 2.00\,mm^3$	$0.75 \times 0.76\,mm^2$	$0.99 \times 1.00 \times 2.00\,mm^3$	$2.98 \times 3.03\,mm^2$	$0.99 \times 1.00 \times 2.20\,mm^3$
Reconstructed resolution	$0.78 \times 0.78 \times 1.00\,mm^3$	$0.59 \times 0.59\,mm^2$	$0.60 \times 0.60 \times 1.00\,mm^3$	$1.04 \times 1.05\,mm^2$	$0.76 \times 0.76 \times 1.10\,mm^3$
Slice thickness (mm)	—	3.00	—	3.00	—
TR/TE (ms)	5.6/2.0/3.8[a]	4134/80	1600/157	4787/78	5.8/2.2/4.0[a]
Preparation/pre-pulse	—	—	$v_{enc} = 1.0\,cm\,s^{-1}$ (CC/RL)	—	—
Diffusion *b* values ($s\,mm^{-2}$)	—	—	—	0, 400, 800	—
FOV (mm^3)	$300 \times 450 \times 300$	$250 \times 450 \times 100$	$250 \times 450 \times 100$	$250 \times 450 \times 100$	$250 \times 425 \times 100$
Acquisition time (m:ss)	4:00	4:33	3:14	3:06	3:10

Abbreviations: TFE = turbo field echo, TSE = turbo spin echo, VISTA = volumetric isotropic T2w acquisition, DWI = diffusion-weighted imaging, FFE = fast field echo, mDixon = multi-point Dixon, SPAIR = spectral attenuated inversion recovery, STIR = short TI inversion recovery, 3D = 3-dimensional, TR = repetition time, TE = echo time, venc = velocity encoding, CC = caudal-cranial, RL = right-left, FOV = field of view.
[a]TR/TE1/TE2.

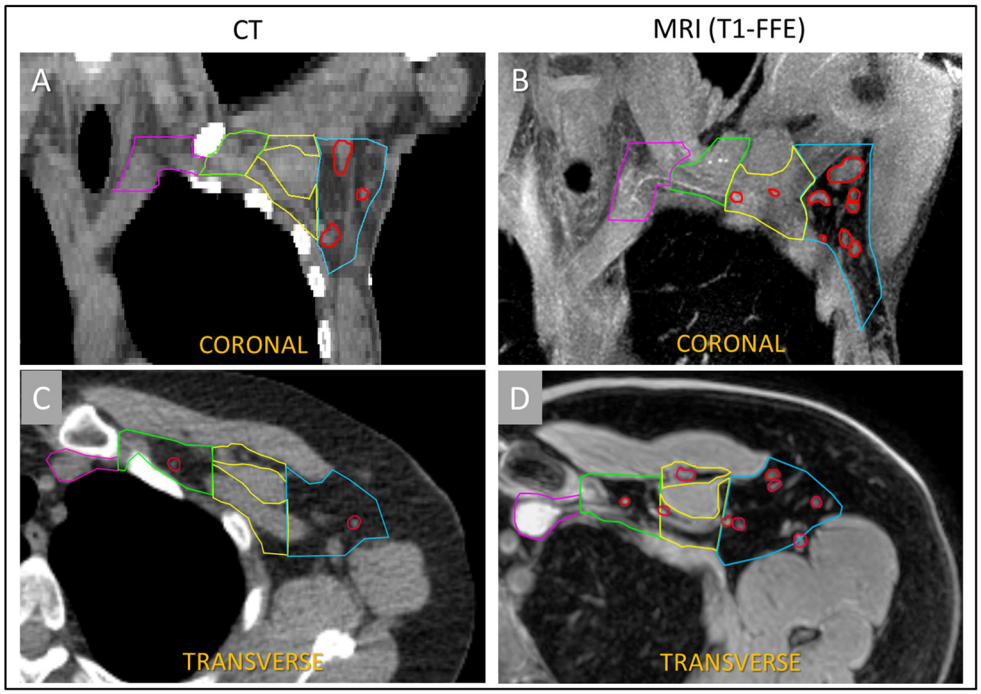

Figure 1. Examples of delineations performed on CT and MRI. CT is shown on the left, (A) and (C), while the Dixon-water image of the T1-FFE MRI scan is shown on the right, (B) and (D). Standard axillary levels I–IV, contoured according to ESTRO guidelines, are depicted in lateral-medial order (in blue: level I, yellow: level II, green: level III, purple: level IV). Individual LNs are also contoured (red).

also applicable for use on MRI. For MRI, minor adaptations were implemented due to soft-tissue differences. We will refer to axillary target contours, defined as levels I–IV, as axillary levels. The interpectoral level was incorporated in level II.

2.6. LN identification and delineation

Using information from all scans in one MRI session, individual LNs were identified, and delineated on the reference scan (figure 1). LN identification was first performed by two observers, who were trained for this by a breast radiologist, and who established an intermediate consensus on structure identifications by using pre- and post-SNB scans. Identification on MRI and CT was validated by two other observers—a breast radiation oncologist and a breast radiologist. After multidisciplinary meetings with all observers, final consensus was reached on pre- and postoperative sets of LNs, on both MRI and CT.

The number of LNs was determined for each patient in scans from both MRI sessions. Moreover, it was determined in which axillary level a LN was located on the preoperative MRI. If an LN was partly located in an axillary level, it was considered to be included in that contour. If an LN was located in more than one level, the level was chosen in which it occupied the greatest volume. Finally, LNs outside the axillary level contours, but within 5 mm, were counted separately. LNs at more than 5 mm distance were excluded. Pre- and

postoperative sets of delineated LNs in each patient were compared on a node-to-node basis. If possible, spatial correlation was established between individual LNs on both MRI sessions.

Furthermore, if possible, the excised SNs were retrospectively identified on the preoperative MRI. This was performed visually, by comparing surrounding LNs and studying anatomical changes. Moreover, the number of excised SNs was taken from the pathology report and compared to differences in the number of LNs before and after SNB. During SNB, SNs excised can also be internal mammary LNs. However, for our analysis we consider only axillary SNs.

The LN detection rate is defined by the number of identified LNs. These were compared per patient, on MRI before and after SNB, while also accounting for the excised SN(s). The postoperative LN detection rate on CT was compared to the postoperative MRI detection rate.

2.7. Statistical analysis

Statistical analysis was performed using *R* software (R Core Team 2014). Normality was checked by visual inspection of calculated Q–Q plots. To assess reproducibility, the LN detection rate on pre-SNB MRI was compared with the LN detection rate on post-SNB MRI using paired Wilcoxon signed-rank tests. Similarly, the LN detection rate of post-SNB MRI was compared to post-SNB CT. Furthermore, Bland-Altman plots were calculated, which represent the difference between the LN detection rates as a function of the average of the two measurements.

2.8. Volumes of LNs and axillary levels

On MRI, the summed volumes of all delineated LNs were determined, in order to indicate potential reduction in target volumes for elective RT, if based on individual LNs instead of entire standard axillary levels. LN-based volumes were compared to volumes of the respective axillary levels. The effect of expanding the LN delineations was also explored by making an isotropic expansion of 5 mm for each individual LN delineation, and performing a similar comparison of the resulting encompassing volume, compared to the axillary levels.

3. Results

3.1. Posture endurance for MRI

Twenty out of 23 patients completed both scan sessions without posture adjustments. One patient experienced pain in her shoulders during both pre- and postoperative MRI. As she was unable to finish either session, not all scans were acquired. Another patient experienced pain in the ipsilateral shoulder, preoperatively, due to a pre-existing cervical hernia. A third patient had a painful contralateral shoulder during postoperative MRI. Patient positioning was adjusted for both of these patients after acquisition of three scans, by lowering the ipsilateral or contralateral arm. The remaining scans were acquired without problems.

3.2. Use of MRI in practice

LNs were visualized in all patients (figures 1 and 2). Fat separation by mDixon was reliable. For LN identification, all acquired MRI scans could be used. In practice not all scans were always contributive. Most LNs were first identified on the T1w SPGR reference scan. The

T2w TSE scans—both showing similar contrast—were consulted to confirm this, and to identify additional LNs, usually close to blood vessels and arteries, due to lack of contrast on T1w images in those locations. A drawback was that image quality of the T2w scans was lower in patients with higher BMI. The other T1w method showed similar contrast as the reference scan and therefore served as confirmation for LN identification. The added value of DWI, while showing some LNs in high contrast, was limited due to low resolution.

3.3. Postoperative artifacts

In all patients, postoperative effects were recognizable on MRI. Enlargement of LNs was observed after SNB in some patients. Repositioning of arteries, muscles and LNs was observed in all patients. Spatial differences related to this were usually small. Formation of postoperative seroma was also visible in all patients, which appeared diluted in all but two patients. The presence of post-SNB effects served as landmarks for retrospectively localizing SNs on preoperative MRI that were excised during SNB (figure 3).

3.4. MRI: detection rates, spatial correlation, and SNs

The median number of LNs was 26 (range: 14–42) on preoperative MRI, and was 25 (range: 13–40) on postoperative MRI (table 3). In total, 617 and 587 LNs were identified, on pre- and post-SNB MRI, respectively. The median number of SNs excised during SNB was 1 (range: 1–3), with a total of 33. For 22 out of 23 patients, the preoperative LN detection rate was equal to the postoperative detection rate on MRI, when the SNs were added ($p = 1.00$) (table 3, figure 4). In one patient, 20 LNs were identified before SNB and 17 after, while 2 SNs had been removed.

In 20 out of the remaining 22 patients, all 550 individual LNs could be spatially correlated between MRI sessions. Any anatomical variation due to a different scanning position did not affect LN correlation in general. In the two other patients, a large postoperative seroma, as well as shifted muscles and arteries, disrupted the anatomy, thereby hampering an exact correlation. However, pre- and postoperative MRI detection rates were equal.

All SNs were identified retrospectively on preoperative MRI. For all patients, numbers of identified SNs matched numbers of excised SNs described in pathology reports (table 3).

3.5. Detection rate on postoperative CT

In total, 255 LNs were identified on all 21 postoperative CT scans. The median number of LNs was 11 (range: 7–22) per patient. LN detection rate on CT was significantly lower than on postoperative MRI ($p < 0.0001$) (table 3, figure 4).

3.6. Relative location of LNs to axillary levels

The majority (353, 57%) of all 617 identified LNs were located in axillary level I (median per patient: 15, range: 13–28) (figure 5). In particular, all 33 identified SNs were identified in level I. The more cranially located an axillary level was, the fewer LNs it tended to contain. A total of 138 (median per patient 6, range: 4–12) LNs were in level II. Only one patient showed more LNs in level II than in level I. Summed over all patients, levels III and IV contained only 42 and 28 LNs respectively (7% and 5%), at a median of 1 LN per patient (ranges: 0–4 and 0–3, respectively). Moreover, 69 LNs (11%) were counted outside the axillary levels, at a

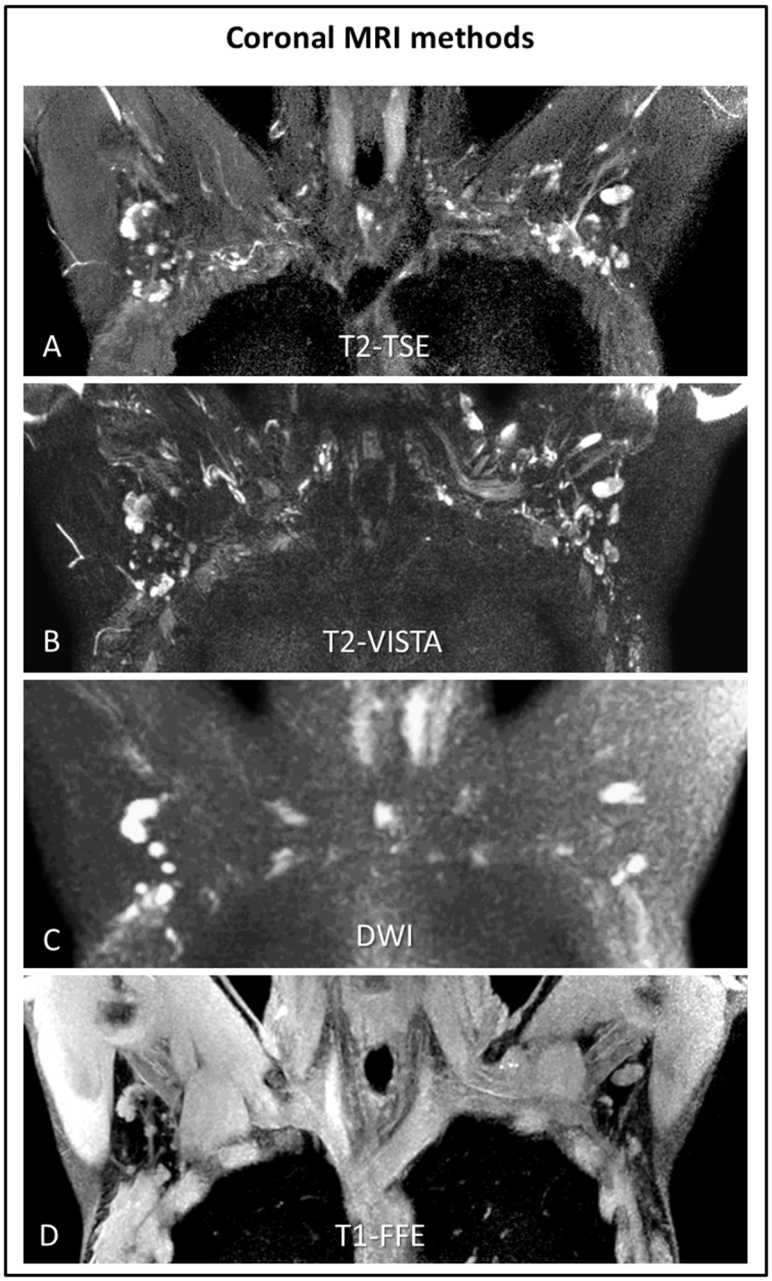

Figure 2. Examples of the four different non-reference MRI scans in one patient, acquired preoperatively in the coronal plane. Individual LNs and surrounding structures are visualized bilaterally. The patient is scanned in supine treatment position, i.e. with both arms in abduction, using T2-TSE ((A), Dixon-water), T2-VISTA (B), DWI ((C), b = 800 s mm^{-2}), and T1-FFE ((D), Dixon-water). These methods were described in more details and evaluated previously (van Heijst *et al* 2016). *Abbreviations:* MRI = magnetic resonance imaging; LNs = lymph nodes; T2-TSE (T2-weighted turbo spin echo; T2-VISTA = T2-weighted volumetric isotropic acquisition; DWI = diffusion-weighted MRI; T1-FFE = T1-weighted fast field echo.

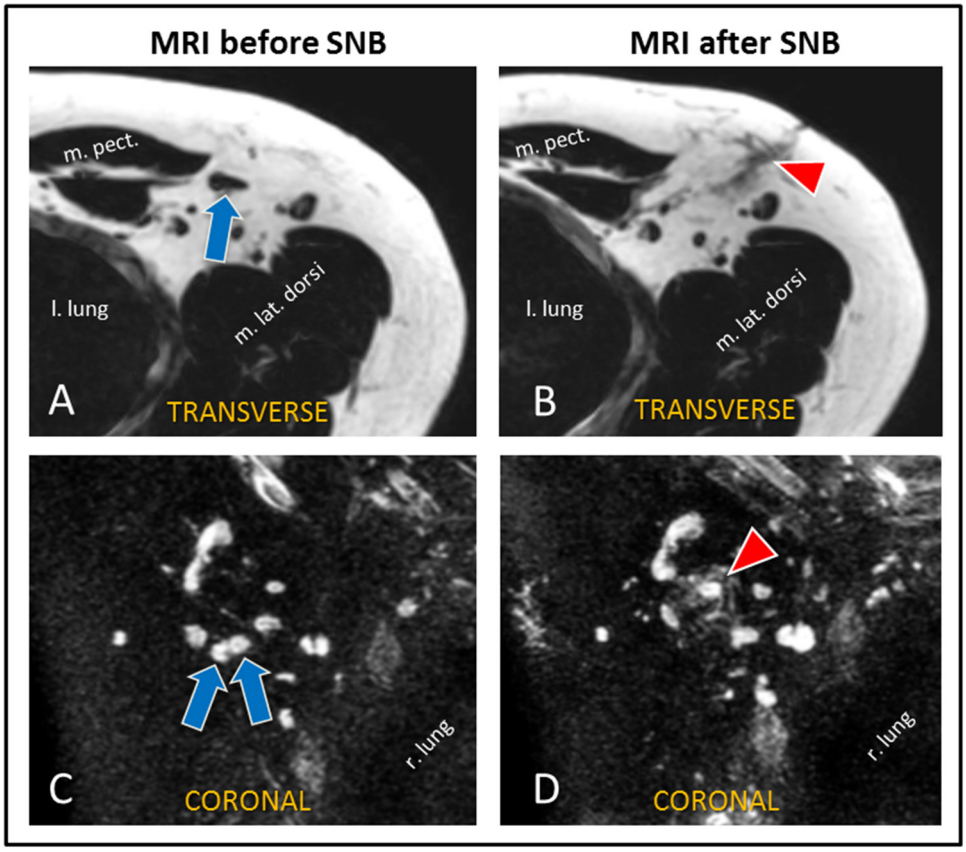

Figure 3. Axillary LNs visualized with MRI before and after SNB. MR images from before SNB (left, (A) and (C)) and after SNB (right, (B) and (D)), in two patients (each row) are depicted. The first row shows Dixon-fat images of a transverse T1-TFE, (A) and (B), where the arrow points to the SN (i.e. absence of fat signal in the SN); the right arrowhead points to postoperative anatomical changes, e.g. presence of seroma. The second example, (C) and (D), is a T2-TSE coronal scan. The blue arrows and red arrowhead similarly show two SNs and postoperative seroma, respectively. *Abbreviations:* SNB = sentinel-node biopsy; m. pect = musculus pectoralis; r. lung = right lung; m. lat. dorsi = latissimus dorsi muscle; l. lung = left lung; T1-TFE = T1-weighted turbo field echo; T2-TSE = T2-weighted turbo spin echo.

median of 2 per patient (range: 0–8). Most of these LNs (49 of 69, 71%) were located nearest to level I.

3.7. LN-based volumes

The summed volume of LNs in level I was the largest, in all patients (table 4). Median LN-based volumes were at most 3% of the volumes of the respective axillary levels. After the 5 mm expansion of each individual LN delineation, the encompassing volume was limited to at most 46% of the corresponding axillary level. The median encompassing volume of LNs counted outside axillary levels on MRI was 5.0 cm^3 after the 5 mm expansion.

Table 3. LN detection rates and numbers of excised SNs. LN detection rates on MRI and CT are listed per individual patient. The number of excised SNs is listed, together with PA value in brackets, denoted as 'number of SNs, PA result'. A value of '—' reflects a tumour-negative SN, while '+' is a tumour-positive SN. Only in patient 12 does 'ΔLNs on MRI' not coincide with the number of axillary SNs from the histopathology reports.

Patient number	Preop MRI	Postop MRI	Postop CT	ΔLNs on MRI	SNs excised (number, ±)
1	28	27	22	1	1 (1, −)
2	42	40	21	2	2 (2, −)
3	35	33	16	2	2 (2, −)
4	24	23	10	1	1 (1, −)
5	34	33	7	1	2 (2, −)[a]
6	33	32	11	1	1 (1, +; macro)
7	19	18	8	1	1 (1, −)
8	23	22	10	1	1 (1, −)
9	21	18	18	3	3 (3, −)
10	28	26	14	2	2 (2, −)
11	23	21	12	2	2 (2, +; isolated cells)
12	20	17	10	3	2 (2, −)
13	33	32	16	1	1 (1, −)
14	26	24	8	2	3 (3, −)[a]
15	26	25	12	1	1 (1, −)
16	17	16	7	1	1 (1, −)
17	20	19	9	1	1 (1, −)
18	26	25	8	1	1 (1, −)
19	14	13	NA	1	1 (1, −)
20	32	31	10	1	1 (1, −)
21	27	26	11	1	1 (1, −)
22	33	32	16	1	1 (1, −)
23	33	32	NA	1	1 (1, −)

Note: LN = lymph node, preop = preoperative, MRI = magnetic resonance imaging, postop = postoperative, CT = computed tomography, ΔLNs = difference in numbers of lymph nodes, SN = sentinel node, PA = pathology, NA = not applicable (since no CT was performed for those patients).

[a] In patients 5 and 14, one SN was an internal mammary LN; it was therefore not counted on preoperative MRI in our analysis.

4. Discussion

MRI of axillary LNs, in supine RT position, is feasible, before and after SNB. Although diagnostic MRI for axillary imaging is thoroughly studied (Lernevall 2000, Harnan *et al* 2011, Rahbar *et al* 2012, Ahmed *et al* 2014, Li *et al* 2014, Menezes *et al* 2014, Kuijs *et al* 2015), MRI studies for target delineation in regional breast RT are scarce.

SNB did not affect patient posture endurance for MRI in supine position. LN detection on MRI scans before and after SNB was highly reproducible, despite postoperative artifacts observed in all patients. All SNs that were excised during SNB were retrospectively identified. Moreover, in 20 patients, all other LNs could be individually correlated between MRI sessions. Compared to MRI, the LN detection rate on CT was significantly lower.

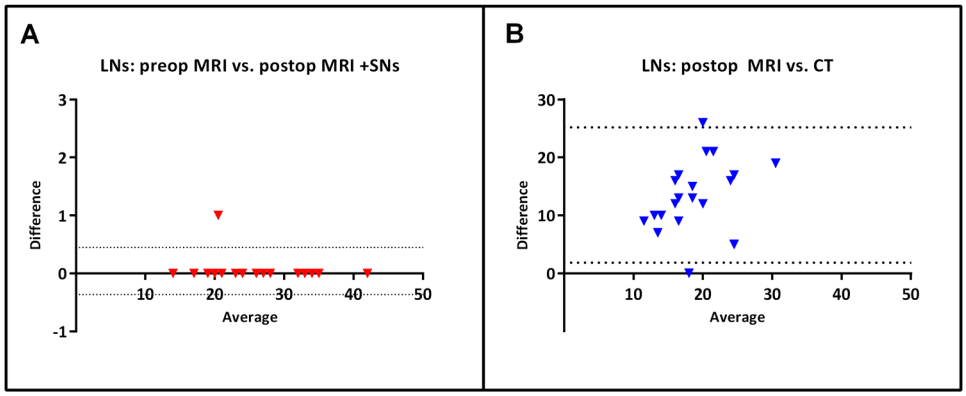

Figure 4. Bland–Altman plots of LN detection rates. Plots are shown for (A) preoperative MRI and postoperative MRI plus number of excised SNs ($n = 23$); (B) postoperative MRI and CT ($n = 21$). These indicate the difference of the two detection rates, as a function of the average of the two measurements. The 95% confidence intervals are indicated by dotted lines.

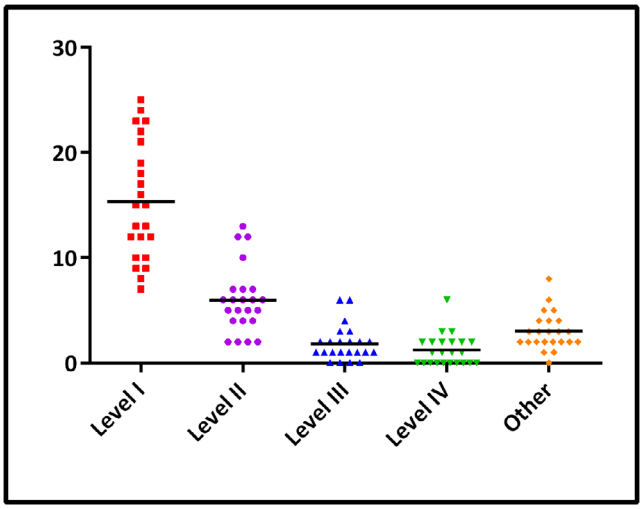

Figure 5. Number of LNs as determined on preoperative MRI for all 23 patients per axillary level. Axillary contours indicated are level I (squares), level II (circles), level III (triangles pointing up), and level IV (triangles pointing down). LNs located outside the axillary levels but within 5 mm distance from the contours are depicted as 'other' (diamonds). Medians are indicated by horizontal lines.

There is no gold standard available for the number of LNs. The numbers in our study, ranging from 14 to 42 on MRI, fall within the expected range of 6–45 LNs, based on previous imaging (MRI, CT, and ultrasonography) and histological studies on LNs (Jiang *et al* 2007, Luciani *et al* 2009, MacDonald *et al* 2010, Korteweg *et al* 2011, Nakai *et al* 2011, Hong *et al* 2012). Histological information, after axillary dissection, is limited to axillary levels I and II, while our work aimed to image LNs in axillary levels I–IV. The range is also similar to that in healthy volunteers (van Heijst *et al* 2016). Most LNs (57%) were located in level I, being the largest axillary volume, including all identified SNs. Two SNs were tumour-positive, but these

Table 4. LN-based target volumes, without and with expansion, per respective axillary level. Volumes based on individual LNs as delineated on MRI are calculated both without expansion (summed volume), and with a 5 mm expansion of each individual LN delineation (encompassing volume). Volumes of respective axillary levels (I–IV) are given, delineated on MRI according to modified ESTRO delineation guidelines (Offersen *et al* 2015). LNs counted outside of the levels are indicated as 'other'. Values are denoted 'median (range)'. Values $< 0.05\,cm^3$ were rounded up to $0.1\,cm^3$. LN = lymph node.

	Summed volume (cm^3)	Encompassing volume (cm^3)	Volume (cm^3)
Location	Individual LNs	Individual LNs (+5 mm each)	Axillary levels
Level I	2.2 (0.9–8.0)	32.8 (16.2–52.5)	71.9 (23.4–162.4)
Level II	0.4 (0.1–0.8)	10.0 (2.9–20.4)	32.0 (17.6–61.7)
Level III	0.1 (0.1–0.3)	3.0 (1.1–10.3)	17.6 (8.8–30.3)
Level IV	0.1 (0.1–0.4)	3.7 (1.4–7.9)	15.4 (11.2–20.7)
Other	0.1 (0.1–0.9)	5.0 (1.7–16.2)	—
Total	3.2 (1.2–9.7)	47.9 (26.7–81.1)	132.8 (69.4–239.8)

were not obviously enlarged on MRI. We did not perform a diagnostic analysis on MRI for the SNs. The more cranially located the level was, the fewer LNs it tended to contain. Numbers of LNs detected in levels III and IV were within the expected range of 1–10 LNs (Ying and Ahuja 2003). However, the supraclavicular region was difficult to image, due to signal from large blood vessels that was not always adequately suppressed in T2w scans, and which could obscure other structures in T1w images. This could have impaired localization of small LNs, possibly hampering the consistency of LN detection on MRI.

The LN detection rate on MRI was significantly higher than on CT, mainly due to its superior soft-tissue contrast. It should be noted that CT was acquired for standard RT target delineation and was not optimized for LN identification.

There are limitations in the set-up of our study. Consensus was reached on LN identification with the expertise of a multidisciplinary team of observers. This did not allow determination of inter-observer variation, as LN identification was performed in consensus, by comparing pre- and postoperative scans together, and in a relatively limited number of patients. Most discussion was on LNs that were located close to blood vessels, the signal of which was not suppressed adequately. This might have led to false positives and false negatives. The current work focused on establishing whether it is feasible to reproduce LN detection before and after SNB, where information from preoperative scans was used in postoperative scans, and vice versa. An inter-observer delineation study will be conducted in the future to assess the potential bias introduced this way. Confirmation of the results in our current study will be investigated in a larger group of patients.

Using ESTRO guidelines (Offersen *et al* 2015) on MRI, up to 8 LNs per patient were located outside the axillary level delineations (but within 5 mm distance), commonly cranial to levels III/IV or dorsolateral to level I. MacDonald *et al* (2010) also found LNs outside axillary levels. The question is whether these LNs should be irradiated. One approach to cover these in the target is to extend the axillary contours (MacDonald *et al* 2010), leading to more treated normal tissue. Indication for current elective RT treatments is determined by results from clinical studies that have investigated anatomical locations of regional recurrences (Offersen *et al* 2013). Delineation guidelines used for regional RT are based on these findings (Nielsen

et al 2013, Offersen *et al* 2013, 2015, Gentile *et al* 2015, Verhoeven *et al* 2015). One could therefore argue that LNs outside the elective axillary levels are not clinically relevant.

The addition of MRI information to standard CT-based RT planning could lead to a more accurate definition of target volumes, by localizing individual LNs. Therefore, we explored individual LN target delineations and calculated LN-based volumes. Even with a 5 mm expansion for each LN delineation, the encompassing volumes are considerably smaller than the respective axillary levels, which are delineated based on vessels and musculature. This signifies that, for elective CT-based RT strategies, adding information from dedicated MRI scans could lead to smaller treated volumes, while still effectively covering the individual LNs.

To implement this into the current clinical CT-based workflow, MRI could be co-registered with the RT-planning CT scan, which could induce set-up variations and registration errors. It is important to perform both scans in the same patient position as much as possible, in order to keep anatomical differences small. Furthermore, the interval between acquisition of the pre-RT MRI and RT-planning CT scans should be as short as possible. Uncertainties due to motion between RT fractions should be minimized. A suitable method could be to use the same dedicated (MRI compatible) positioning device on both CT and MRI modalities, and on the linear accelerator. The impact of any remaining errors due to inter-fraction motion should be quantified. However, the potential clinical benefit of adding MRI in the current clinical process is high.

As shown in our study, significantly more LNs are found on MRI than on CT. Moreover, they are imaged in a direct relationship to surrounding radiosensitive structures, e.g. the heart, brachial plexus, and chest wall. The RT planning volume could be adapted accordingly by restricting the RT dose more conformally to the LNs, thereby sparing healthy tissue, decreasing the overall treated volume, and potentially reducing toxicity. Furthermore, nowadays, elective RT of LNs is performed after axillary surgery. Since the presence of postoperative artifacts could obscure LNs, new approaches may focus on preoperative RT instead.

On-line MRI guidance, as achieved by the UMC Utrecht MRI/linear accelerator and other MRI/RT modalities (Dempsey *et al* 2006, Lagendijk *et al* 2008, Fallone *et al* 2009, Raaymakers *et al* 2009) could be beneficial for LN-based RT treatments by reducing set-up uncertainties, as ideally this is performed in an MRI-only workflow. Moreover, the clinical availability of these hybrid MRI/RT modalities could open further possibilities for treatment approaches of individual LNs, such as the delivery of a stereotactic high dose to tumour-positive LNs. For such advanced stereotactic RT techniques, the use of additional methods for identifying metastatic LNs on MRI is necessary (Harnan *et al* 2011). Such novel approaches may lead to lower RT-related toxicity, shorter RT treatment schedules, or omission of surgery for selected breast cancer patients. The feasibility of MRI-guided RT, specifically targeting individual LNs, is currently under investigation at UMC Utrecht.

5. Conclusion

MRI of LNs in supine RT position in breast cancer patients is feasible. The LN detection rate on MRI is reproducible before and after SNB. Implementation of MRI in RT planning may lead to more accurate target definition, compared to CT-based regional RT planning. LN-based delineation using MRI may result in a reduction in standard regional RT target volumes. This may facilitate new regional RT approaches in breast cancer patients targeting individual LNs.

ORCID iDs

Tristan C F van Heijst https://orcid.org/0000-0001-8493-8247

References

Ahmed M, Usiskin S I, Hall-Craggs M A and Douek M 2014 Is imaging the future of axillary staging in breast cancer? *Eur. Radiol.* **24** 288–93

Dempsey J, Dionne B, Fitzsimmons J, Haghigat A, Li J, Low D, Mutic S, Palta J, Romeijn H and Sjoden G 2006 WE-E-ValA-06: a real-time MRI guided external beam radiotherapy delivery system *Med. Phys.* **33** 2254

Dijkema I M, Hofman P, Raaijmakers C P J, Lagendijk J J, Battermann J J and Hillen B 2004 Loco-regional conformal radiotherapy of the breast: delineation of the regional lymph node clinical target volumes in treatment position *Radiother. Oncol.* **71** 287–95

Donker M *et al* 2014 Radiotherapy or surgery of the axilla after a positive sentinel node in breast cancer (EORTC 10981–22023 AMAROS): a randomised, multicentre, open-label, phase 3 non-inferiority trial *Lancet Oncol.* **15** 1303–10

Eggers H, Brendel B, Duijndam A and Herigault G 2011 Dual-echo Dixon imaging with flexible choice of echo times *Magn. Reson. Med.* **65** 96–107

Fallone B G, Murray B, Rathee S, Stanescu T, Steciw S, Vidakovic S, Blosser E and Tymofichuk D 2009 First MR images obtained during megavoltage photon irradiation from a prototype integrated linac-MR system *Med. Phys.* **36** 2084–8

Galimberti V *et al* 2013 Axillary dissection versus no axillary dissection in patients with sentinel-node micrometastases (IBCSG 23-01): a phase 3 randomised controlled trial *Lancet Oncol.* **14** 297–305

Gentile M S, Usman A A, Neuschler E I, Sathiaseelan V, Hayes J P and Small W 2015 Contouring guidelines for the axillary lymph nodes for the delivery of radiation therapy in breast cancer: evaluation of the RTOG breast cancer atlas *Int. J. Radiat. Oncol. Biol. Phys.* **93** 257–65

Giuliano A E, McCall L, Beitsch P, Whitworth P W, Blumencranz P, Leitch A M, Saha S, Hunt K K, Morrow M and Ballman K 2010 Locoregional recurrence after sentinel lymph node dissection with or without axillary dissection in patients with sentinel lymph node metastases: the American College of Surgeons Oncology Group Z0011 randomized trial *Ann. Surg.* **252** 12–21

Hadamitzky C, Spohr H, Debertin A S, Guddat S, Tsokos M and Pabst R 2010 Age-dependent histoarchitectural changes in human lymph nodes: an underestimated process with clinical relevance? *J. Anat.* **216** 556–62

Harnan S E, Cooper K L, Meng Y, Ward S E, Fitzgerald P, Papaioannou D, Ingram C, Lorenz E, Wilkinson I D and Wyld L 2011 Magnetic resonance for assessment of axillary lymph node status in early breast cancer: A systematic review and meta-analysis *Eur. J. Surg. Oncol.* **37** 928–36

Hong Y, Xiang L, Hu Y, Zhou Z, Yu H and Zhu B 2012 Interstitial magnetic resonance lymphography is an effective diagnostic tool for the detection of lymph node metastases in patients with cervical cancer *BMC Cancer* **12** 360

Jiang J, He Q, Yang X, Liang Y, Fan L J, Zhang Y and Guo M Q 2007 Contribution of minute axillary lymph nodes to accurate staging for patients with breast cancer *Chin. Med. J.* **120** 1762–5 (PMID: 18028767)

Korteweg M A, Zwanenburg J J M, Hoogduin J M, van den Bosch M A A J, van Diest P J, van Hillegersberg R, Eijkemans M J C, Mali W P T M, Luijten P R and Veldhuis W B 2011 Dissected sentinel lymph nodes of breast cancer patients: characterization with high-spatial-resolution 7-T MR imaging *Radiology* **261** 127–35

Kuijs V J L, Moossdorff M, Schipper R J, Beets-Tan R G H, Heuts E M, Keymeulen K B M I, Smidt M L and Lobbes M B I 2015 The role of MRI in axillary lymph node imaging in breast cancer patients: a systematic review *Insights Imaging* **6** 203–15

Lagendijk J J W, Raaymakers B W, Raaijmakers A J E, Overweg J, Brown K J, Kerkhof E M, van der Put R W, Hårdemark B, van Vulpen M and van der Heide U A 2008 MRI/linac integration *Radiother. Oncol.* **86** 25–9

Lernevall A 2000 Imaging of axillary lymph nodes *Acta Oncol.* **39** 277–81

Li C, Meng S, Yang X, Wang J and Hu J 2014 The value of T2∗ in differentiating metastatic from benign axillary lymph nodes in patients with breast cancer—a preliminary *in vivo* study *PLoS One* **9** e84038

Luciani A *et al* 2009 *Ex vivo* MRI of axillary lymph nodes in breast cancer *Eur. J. Radiol.* **69** 59–66

Luscieti P, Hubschmid T, Cottier H, Hess M W and Sobin L H 1980 Human lymph node morphology as a function of age and site *J. Clin. Pathol.* **33** 454–61

MacDonald S M, Harisinghani M G, Katkar A, Napolitano B, Wolfgang J and Taghian A G 2010 Nanoparticle-enhanced MRI to evaluate radiation delivery to the regional lymphatics for patients with breast cancer *Int. J. Radiat. Oncol. Biol. Phys.* **77** 1098–104

Menezes G L, Knuttel F M, Stehouwer B L, Pijnappel R M and van den Bosch M A 2014 Magnetic resonance imaging in breast cancer: a literature review and future perspectives *World J. Clin. Oncol.* **5** 61–70

Nakai G, Matsuki M, Harada T, Tanigawa N, Yamada T, Barentsz J and Narumi Y 2011 Evaluation of axillary lymph nodes by diffusion-weighted MRI using ultrasmall superparamagnetic iron oxide in patients with breast cancer: initial clinical experience *J. Magn. Reson. Imaging* **34** 557–62

Nielsen M H *et al* 2013 Delineation of target volumes and organs at risk in adjuvant radiotherapy of early breast cancer: national guidelines and contouring atlas by the Danish Breast Cancer Cooperative Group *Acta Oncol.* **52** 703–10

Offersen B V, Nielsen H M, Overgaard M and Overgaard J 2013 Is regional nodes radiotherapy an alternative to surgery? *Breast* **22** S118–28

Offersen B V *et al* 2015 ESTRO consensus guideline on target volume delineation for elective radiation therapy of early stage breast cancer *Radiother. Oncol.* **114** 3–10

Raaymakers B W *et al* 2009 Integrating a 1.5 T MRI scanner with a 6 MV accelerator: proof of concept *Phys. Med. Biol.* **54** N229–37

Rahbar H, Partridge S C, Javid S H and Lehman C D 2012 Imaging axillary lymph nodes in patients with newly diagnosed breast cancer *Curr. Probl. Diagn. Radiol.* **41** 149–58

R Core Team 2014 R: a language and environment for statistical computing *R Found Statistical Computing* vol 0 (Vienna, Austria)

Srivastava V, Basu S and Shukla V K 2012 Seroma formation after breast cancer surgery: what we have learned in the last two decades *J. Breast Cancer* **15** 373–80

van Heijst T C F, van Asselen B, Pijnappel R M, Cloos-van Balen M, Lagendijk J J W, van den Bongard H J G D and Philippens M E P 2016 MRI sequences for the detection of individual lymph nodes in regional breast radiotherapy planning *Br. J. Radiol.* **89** 20160072

Verhoeven K *et al* 2015 Vessel based delineation guidelines for the elective lymph node regions in breast cancer radiation therapy—PROCAB guidelines *Radiother. Oncol.* **114** 11–6

Ying M and Ahuja A 2003 Sonography of neck lymph nodes. Part I: normal lymph nodes *Clin. Radiol.* **58** 351–8